

Multiple-Peak Selection Surface Simulation Methods

Diogo, Miudo, Gabriel, (não sei mais quem)

07/03/2024

Summary

Applying the dynamics predicted by the Lande equation, we use numeric simulations to investigate how a population with a fixed G-matrix evolves on a complex fitness landscape. We show that under certain conditions related to the number and position of the adaptive peaks, the G-matrix can alter the macroevolutionary history of a population. In particular, in a multiple peak landscape, the final phenotype of the population can be altered by G-matrix, and this effect produces an observable signature in the divergence between species.

Introduction

This document is a supporting information annex to “Bridging the gap...”. Here, we describe in detail the simulations used to study the interaction between differing levels of genetic integration and complex selective surfaces. Our objective here is to study how these two parameters, genetic variation and selective surface, affect the relation between vector of phenotypic change and the genetic covariation in the population. There are two main elements to the simulations: (1) The level of integration in the genetic covariance matrix of the population under selection; and (2) the ruggedness, or number of peaks, of the selective surface. We begin by developing a strategy to simulate simple and complex selective surfaces.

The selective surface

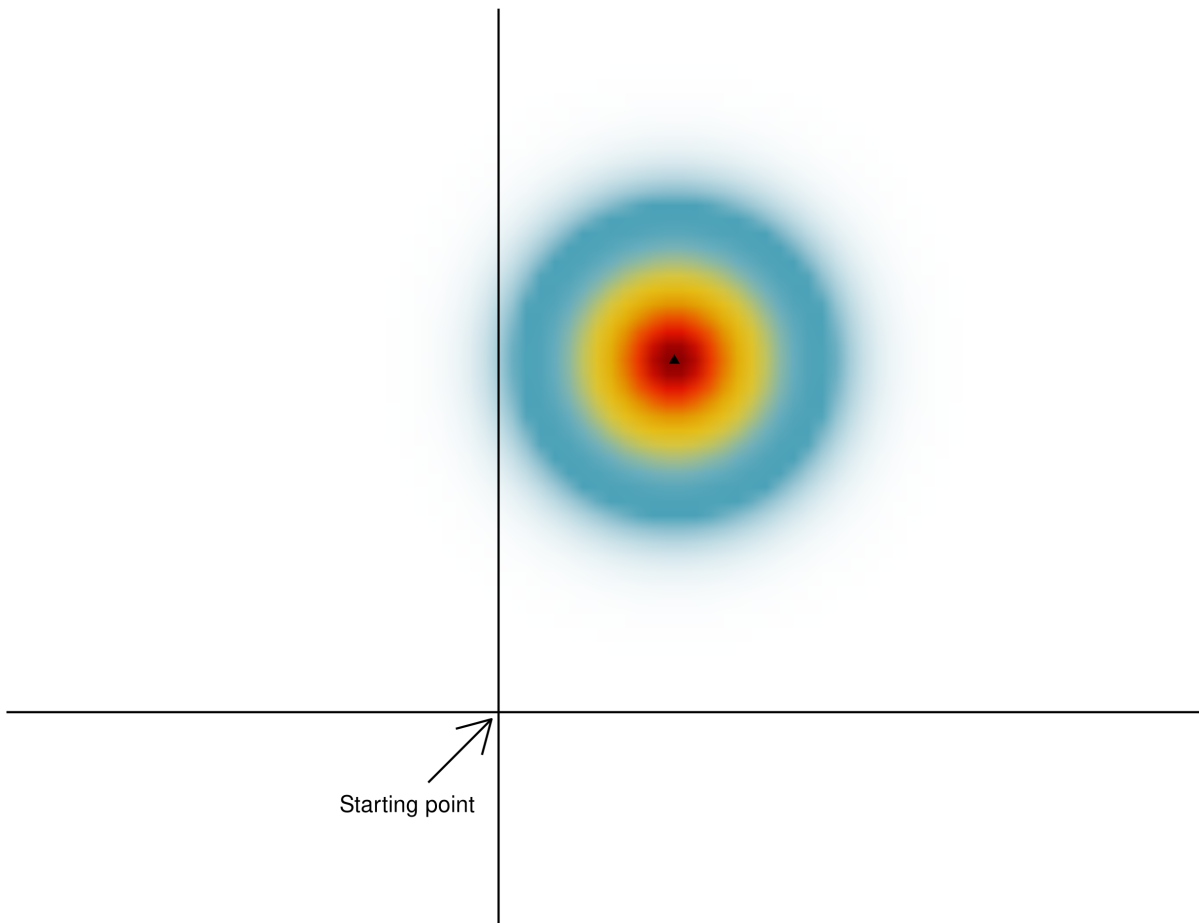
We are interested in creating both very simple selective surfaces, with only a single phenotypic optimum for the population, and complex surfaces, with several optima distributed across the phenotypic space. In order to achieve this, we use a mixture of Gaussian functions. For the single peak landscape, we can simply sample a multivariate mean θ from some random distribution and use the diagonal matrix (Σ) as a covariance for the multivariate normal¹. This induces the following mean fitness surface, for a k -dimensional phenotype x :

$$\bar{W}(x) = \mathcal{N}(x|\theta, \Sigma) = \det(2\pi\Sigma)^{-\frac{1}{2}} e^{-\frac{1}{2}(x-\theta)^T \Sigma^{-1} (x-\theta)}$$

For a bivariate phenotype, we can visualize this surface using a color gradient (SI Fig 1). The triangle marks the position of the θ parameter. The origin of the coordinate system marks where our populations will be in relation to the selective surface.

Creating more complex surfaces can follow basically the same strategy, but using several overlapping Gaussian functions. For this, we have to sample several θ parameters and define the fitness as the sum of all the Gaussian functions. For a set of N Gaussian, each with a different θ and the same Σ , we have:

¹The Σ parameter could be any positive definite matrix, but we do not explore this parameter here, and use the identity matrix in all simulations.



SI Figure 1: Single peak surface. The triangle marks the position of the θ parameter. The origin of the coordinate system marks where our populations will be in relation to the selective surface.

$$\bar{W}(x) = \sum_{i=1}^N \mathcal{N}(x|\theta_i, \Sigma) = \det(2\pi\Sigma)^{-\frac{1}{2}} \sum_{i=1}^N e^{-\frac{1}{2}(x-\theta_i)^T \Sigma^{-1}(x-\theta_i)}$$

In order to sample the θ parameters for the Gaussian functions, we could use uniform distributions in some interval to sample the (x, y) components for several optima, like in SI Fig 2. However, this causes problems in relation to the origin, as some directions have more peaks than others. The directions along the diagonals are longer than along the two axes, and so we end up with more peaks along the diagonals. One solution is to sample the (x, y) components from a normal distribution, which is spherically symmetrical, and then scale the resulting vectors to a magnitude sampled from a uniform distribution. This gives us control over the distance of the peaks from the origin and guarantees that all directions are equally likely, as in SI Fig 3. This procedure also generalizes to more dimensions, and avoids the problem of having all the peaks in a thin shell in multivariate space that would happen if we were to only sample all coordinates from a normal distribution and not sample the magnitudes separately.

The final restriction on the multiple peaks is to impose a minimum distance from the origin. This is necessary so that our population can actually evolve, and not start the simulation already at a phenotypic optima. We do this by restricting the distance of the Gaussian optima to be larger than some minimum distance. A set of θ parameters that follow these rules is displayed in SI Fig 4, and this particular set of θ results in the complex surface shown in SI Fig 5. We can see that the optima for the full surface don't necessarily coincide with one particular θ and that this method can create complex surfaces, with several peaks, valleys, ridges, and saddle points.

Interaction between genetic covariation and the selective surface

After we have created a surface, we can place a population at any point and use quantitative genetics theory to predict how the mean phenotype of the population will change over time. Assuming the additive genetic covariance matrix of the population (G -matrix) stays constant, at each generation the change in the mean phenotype Δz will be given by the Lande equation:

$$\Delta z = G\beta = G \frac{1}{\bar{W}} \nabla \bar{W} = G \nabla \ln \bar{W}$$

In this equation, the selection vector (β) is given by the gradient of the natural logarithm of the selective surface. The choice of modeling the selective surface with a sum of Gaussian functions allows for an analytical calculation of the gradient, which greatly improves the efficiency of the simulations. Using numerical gradients would make simulations in high dimensional cases impossible.

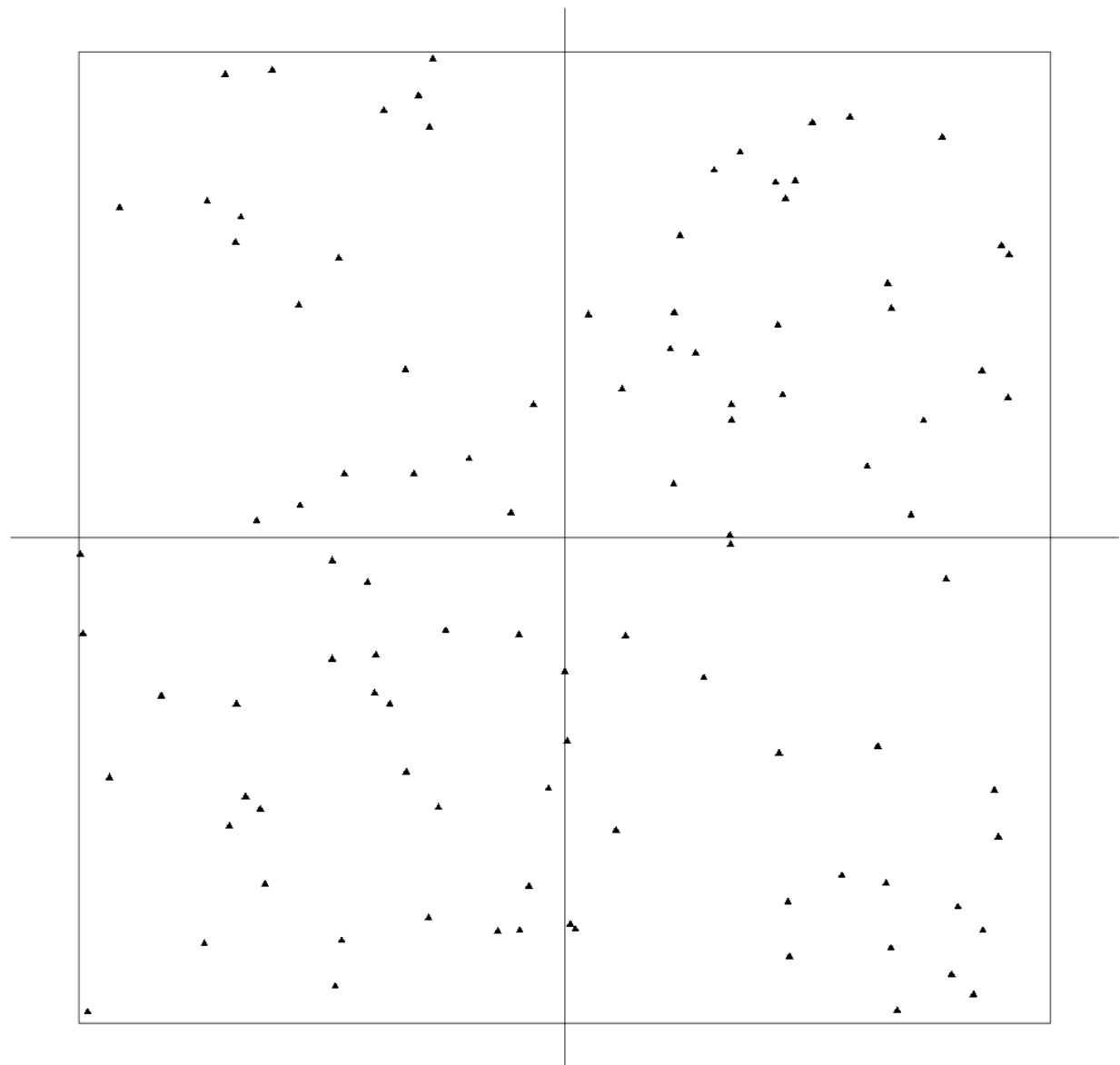
For a single multivariate Gaussian function $p(x|\theta, \Sigma)$, with $x \in \mathbb{R}^k$, the gradient of $p(x|\theta, \Sigma)$ is given by:

$$\frac{\partial p(x|\theta, \Sigma)}{\partial x} = -p(x)\Sigma^{-1}(x - \theta)$$

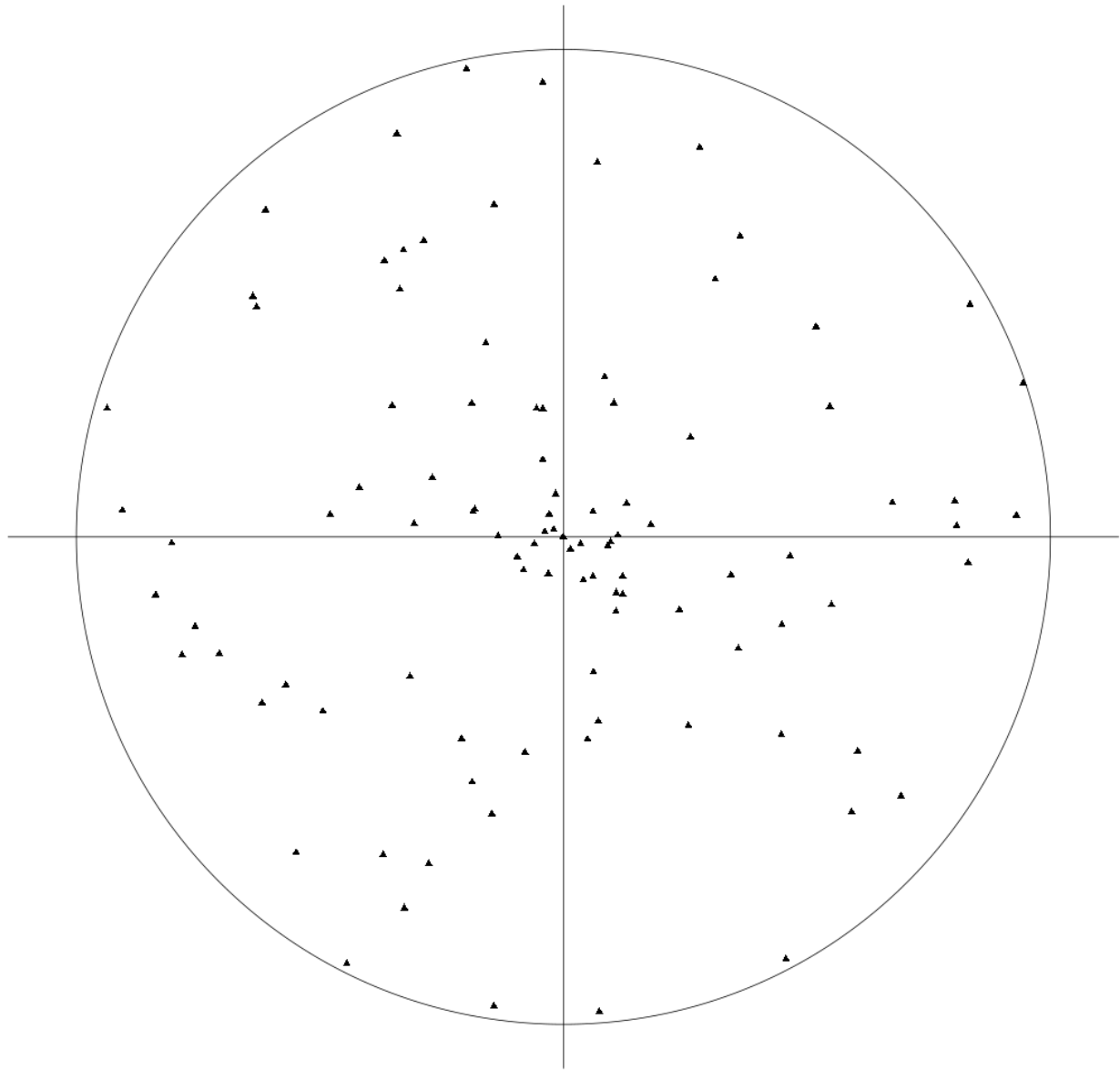
For a complex surface defined as the sum of several Gaussian functions, with $p_i(x) = p(x|\theta_i, \Sigma)$, $\bar{W}(x|\theta_1, \dots, \theta_n, \Sigma) = \sum_{i=1}^n p_i(x)$, the gradient of the logarithm of $\bar{W}(x)$ is given by:

$$\nabla \ln \bar{W}(x|\theta_1, \dots, \theta_n, \Sigma) = \frac{1}{\bar{W}(x)} \sum_{i=1}^n -p_i(x)\Sigma^{-1}(x - \theta_i)$$

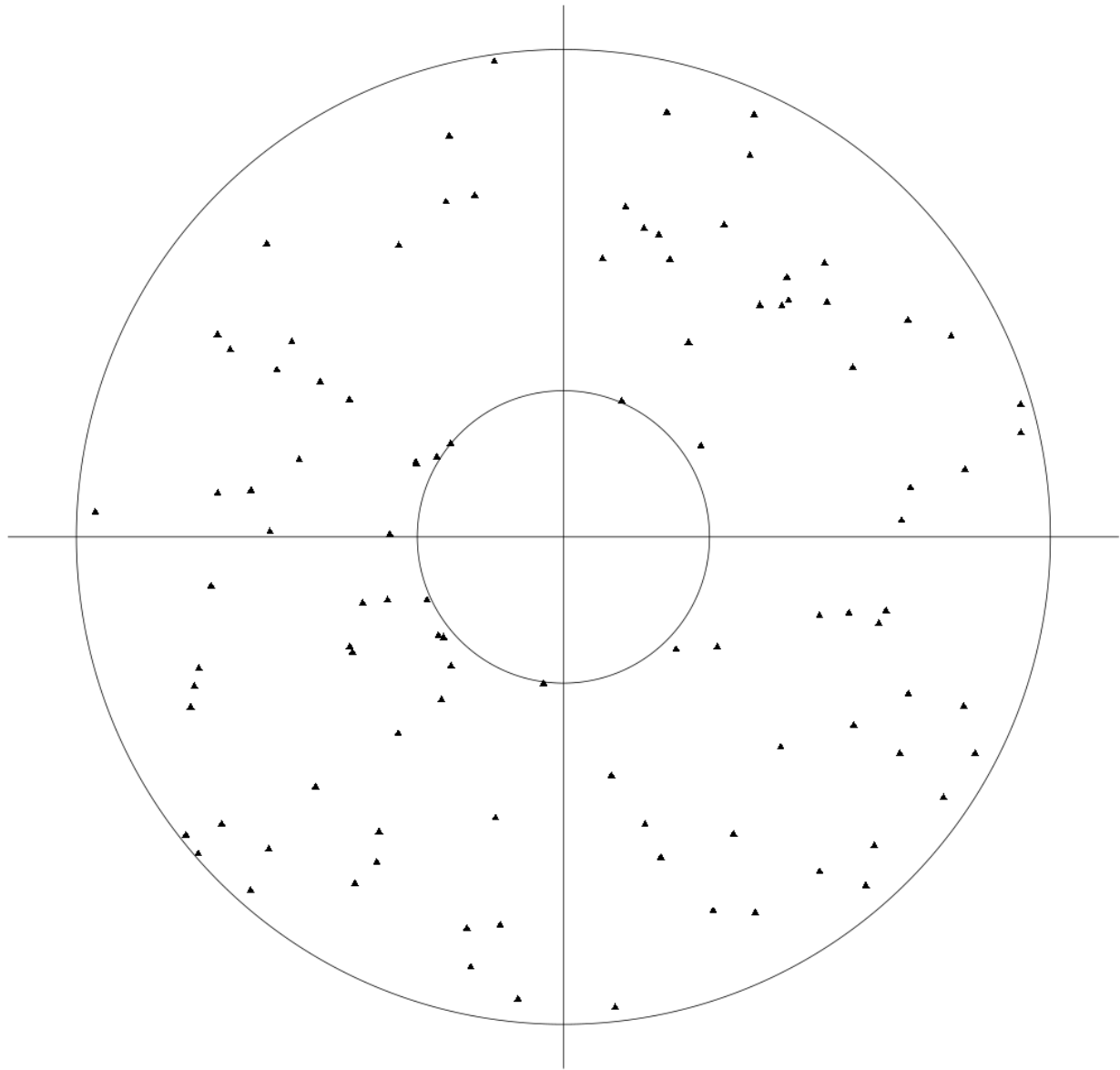
Multiplying the gradient at the position the population currently occupies by the G -matrix gives the phenotypic change, which can be added to the current position to obtain the new position of the population after selection. Iterating this process gives a trajectory in phenotype space, which stops when the gradient is zero. Different covariance matrices will create different trajectories. For example, SI Fig 6 shows the difference between the trajectories of two populations with high and low integration. In this example, both populations end up on the



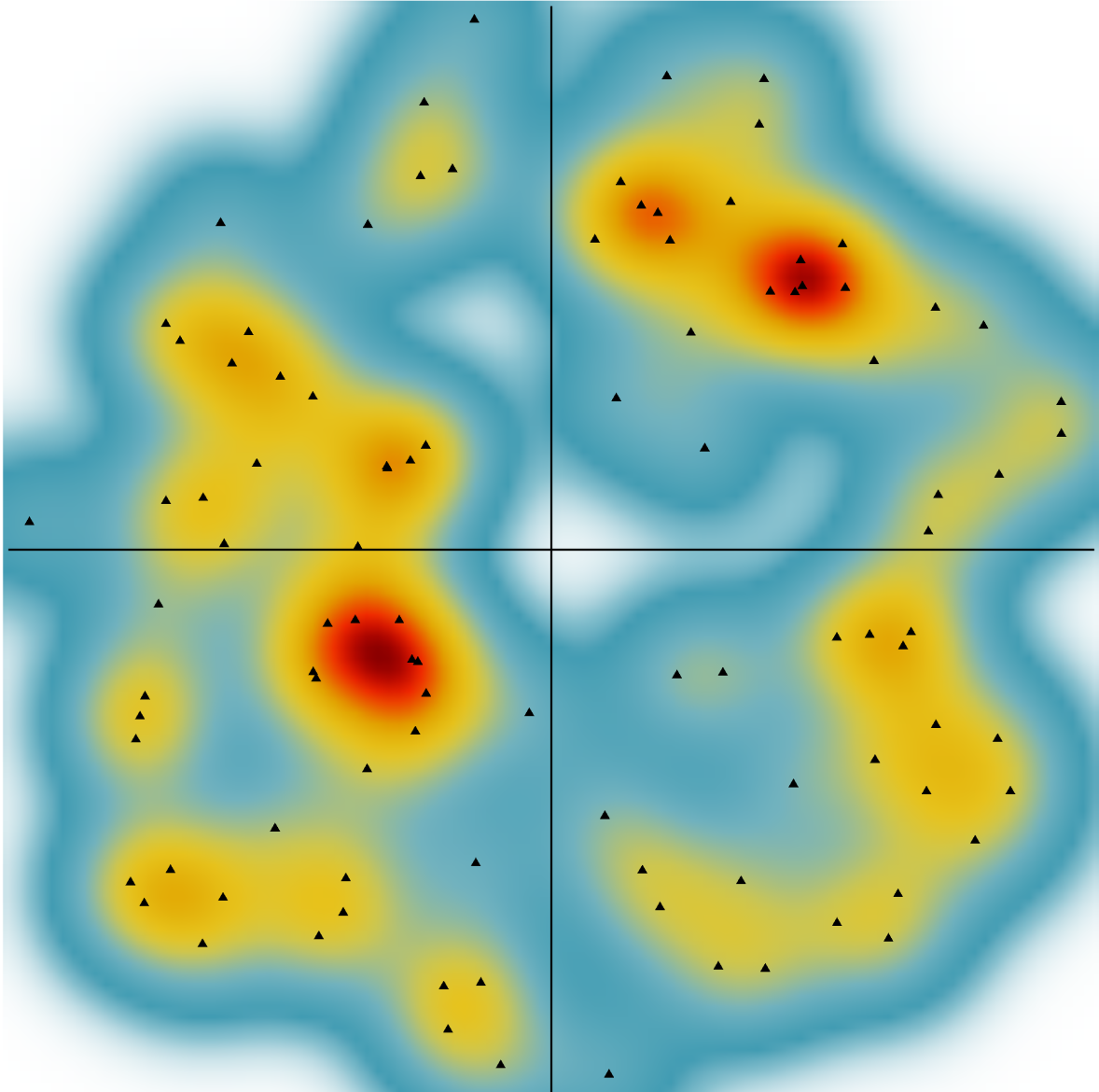
SI Figure 2: Multiple Gaussian optima with uniform coordinates. All the peaks are restricted to be inside the square, but this causes a bias in direction in relation to the origin. Directions along the diagonal are longer, and so have more peaks along them.



SI Figure 3: Multiple Gaussian optima with spherical symmetry and uniform distance from origin.

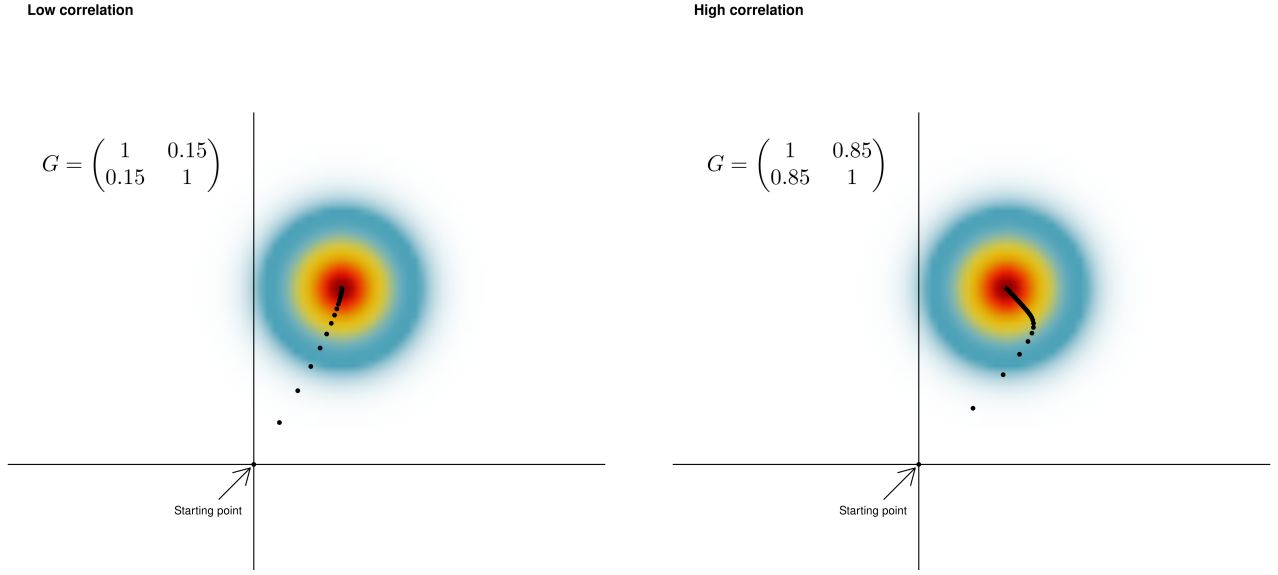


SI Figure 4: Multiple Gaussian optima with spherical symmetry and a minimum distance from the origin.



SI Figure 5: Surface generated by the multiple Gaussian optima in SI Fig 4.

same optimum. However, if the surface is more complex, with several optima, they can end up on different optima. SI Fig 7 shows a slightly more complex surface where the different correlations lead the populations to different optima on the same surface. As the surfaces become more complex, these cases become more frequent.



SI Figure 6: Different G-matrices produce different trajectories for the surface in SI Fig 1.

Simulations

We use this framework of generating random selective surfaces to investigate the relation between the magnitude of the total phenotypic change ($\|\Delta z\|$) and evolutionary bias: the alignment between the direction of phenotypic change and the main axis of genetic variation in the populations (given by the cosine of the angle between these vectors: $\text{Cos}(g_{max}, \Delta z)$, see SI Fig 8).

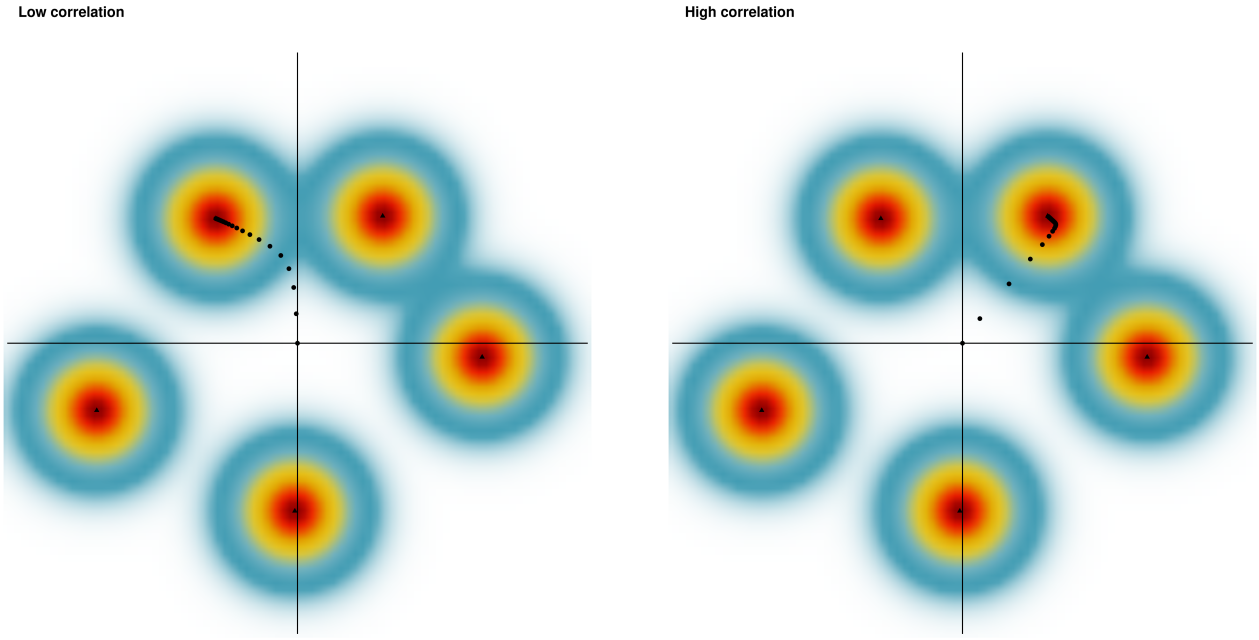
We use 4 different scenarios, presenting high and low integration populations with single- and multi-peaked selective surfaces. By generating several different surfaces, we can investigate the relation between these variables.

Covariance matrices

In order to generate simulations that are comparable to the empirical results, we used one of the empirical P-matrices as a hypothetical G-matrix in our simulations. We use a very highly integrated P-matrix, from the marsupial order Lutreolina, as the **high-integration** G-matrix in our simulations (eigenvalue variance=0.55). To create a comparable low-integration matrix, we start with the high-integration matrix and alter the distribution of variance among the eigenvalues in order to modify the integration, while keeping the eigenvectors and total variation constant. This is done by exponentiating the eigenvalues by some constant p and multiplying them by a scaling factor s . If G_H is the original high-integration matrix, λ_{G_H} and Λ_{G_H} are respectively its eigenvalues and eigenvectors, the new low-integration matrix has the form:

$$G_{new} = \Lambda_{G_H} s \lambda_{G_H}^p \Lambda_{G_H}^{-1}$$

If p is greater than one, the variance in the eigenvalues increases and consequently the overall magnitude of genetic integration also increases. If p is less than one, the variance of the eigenvalues is reduced, and so is the integration.



SI Figure 7: Different G-matrices can alter the final position in the landscape.

We chose the value of p by targeting an integration value below 0.01, which is lower than most empirical matrices. This value is calculated using the standardized eigenvalue variance described in Machado et al. 2019, using the CalcEigenVar function in the evolqg package. The scaling factor s is chosen so that this new matrix has the same total variance as the original matrix (Lutreolina).

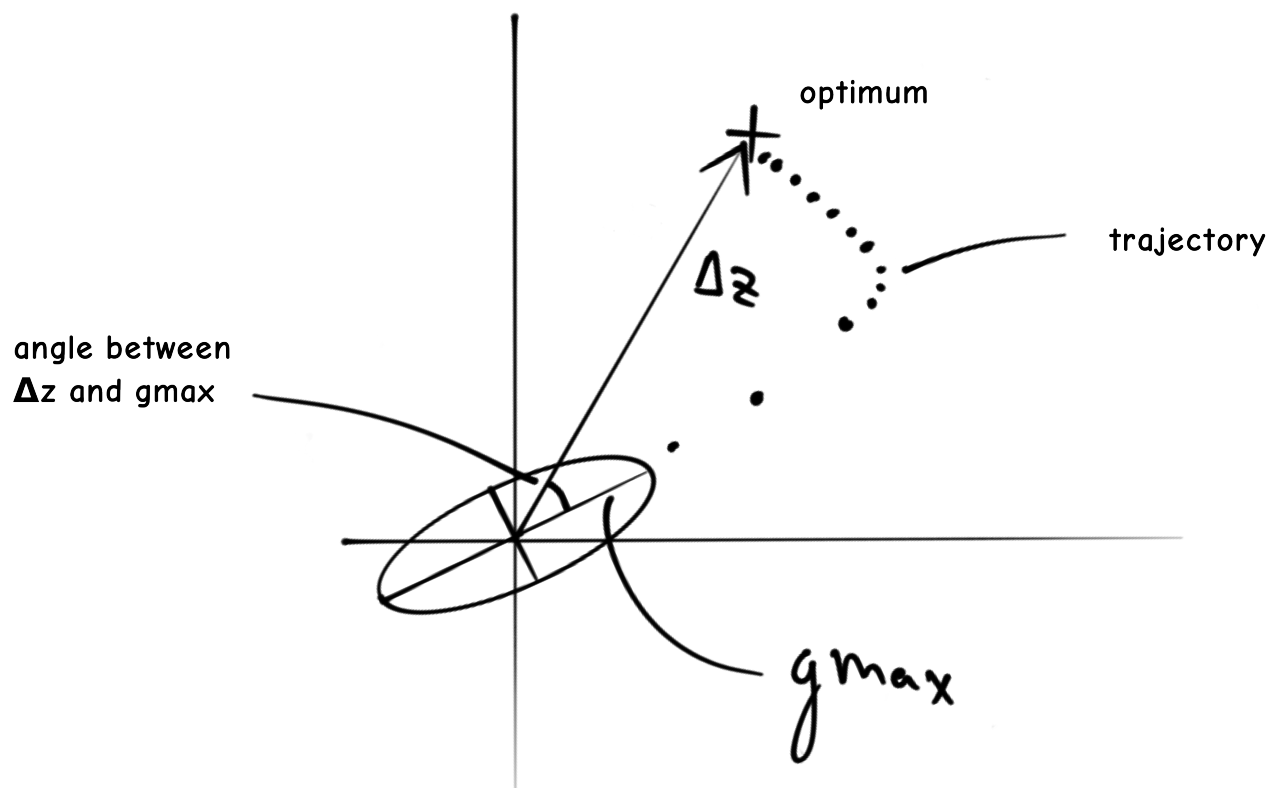
Random peaks

We start the simulation by using randomly generated peaks, as shown in SI Fig 5. For the single peak landscapes, there is no difference between high- and low-integration matrices, and $\|\Delta z\|$ values are widely distributed for both matrices, with large and small amounts of phenotypic divergence being equally likely. We observe no relation between $\|\Delta z\|$ and $\text{Cor}(\Delta z, g_{max})$ (SI Fig 9). The multi peak landscape leads to much less variation in $\|\Delta z\|$, with most values clustering around the minimum peak distance for both matrices. Again, there is no influence of $\text{Cor}(\Delta z, g_{max})$ on $\|\Delta z\|$.

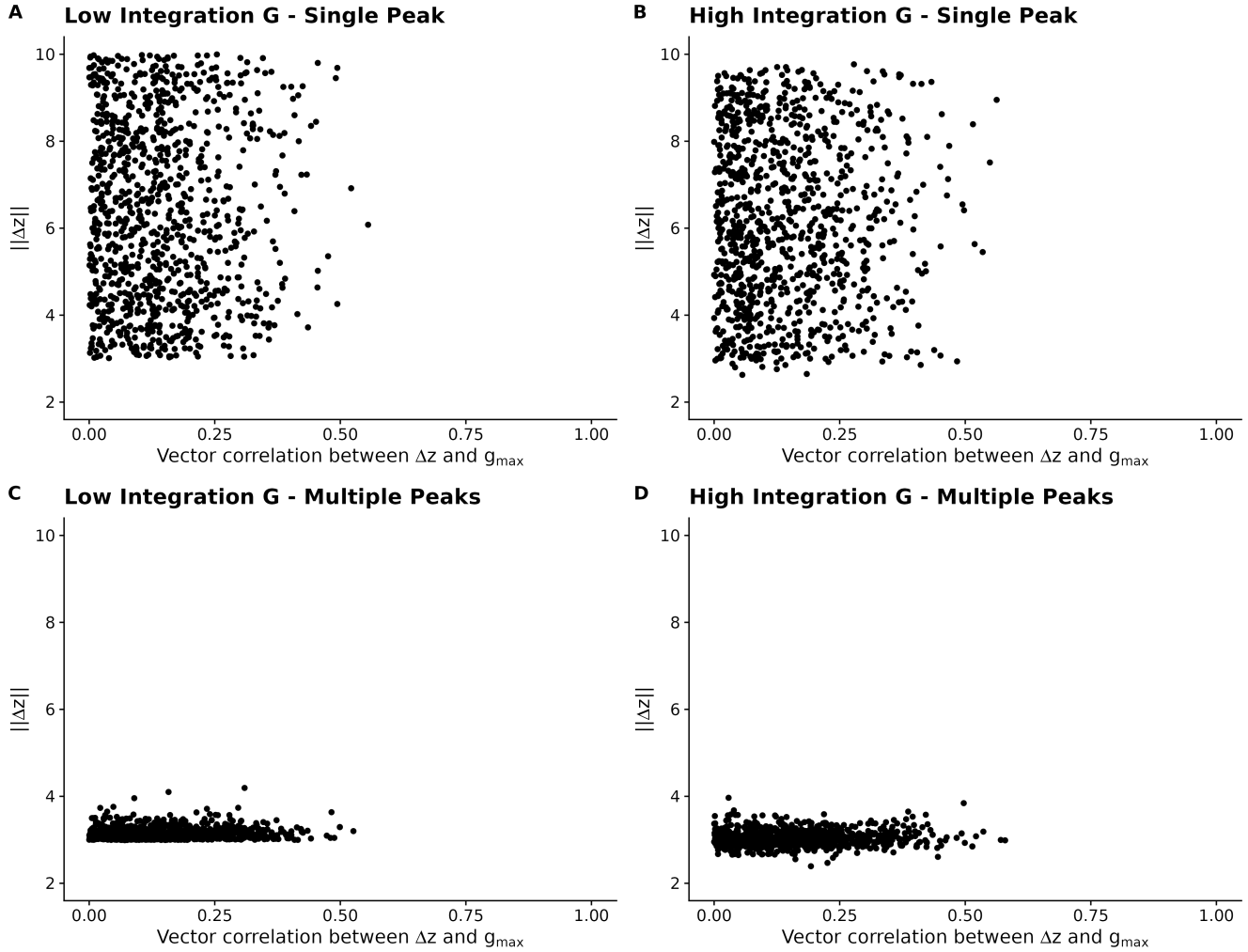
There is a conspicuous absence of $\text{Cor}(\Delta z, g_{max})$ values above 0.6. This is a problem because this is exactly the parameter region we expect to lead to differences in $\|\Delta z\|$. The lack of any peaks in this region of the phenotypic space can be explained by the high dimensionality of the system. The probability that random vectors in high dimensional space will have a correlation above 0.6 is vanishingly small. Thus, this adaptive landscape, with randomly placed peaks, would be the equivalent of having no adaptive peaks whatsoever aligned with the G-matrix. We address this by slightly modifying the distribution of peaks.

Enriched peaks

To effectively sample the region of phenotype space that is aligned with g_{max} , we developed a sampling procedure that enriches the peaks in the direction of g_{max} to a customizable amount. The idea is to sample random vectors in a way that produces a set of peaks that are in directions correlated with g_{max} according to a predetermined target distribution of $\text{Cor}(\Delta z, g_{max})$. To create this target distribution, we start by establishing the distribution of $\text{Cor}(\Delta z, g_{max})$ under a random sampling of peaks. This random distribution can be adequately represented by a beta distribution $Beta(a, b)$, which we fit to the observed random correlations using maximum likelihood, obtaining



SI Figure 8: Scheme of the measurements in a simulation run. The total length of the phenotypic change is given by the norm of the Δz vector. The angle between the direction of most genetic variation (g_{max}) and the Δz vector measures the alignment between phenotypic change and genetic variation.

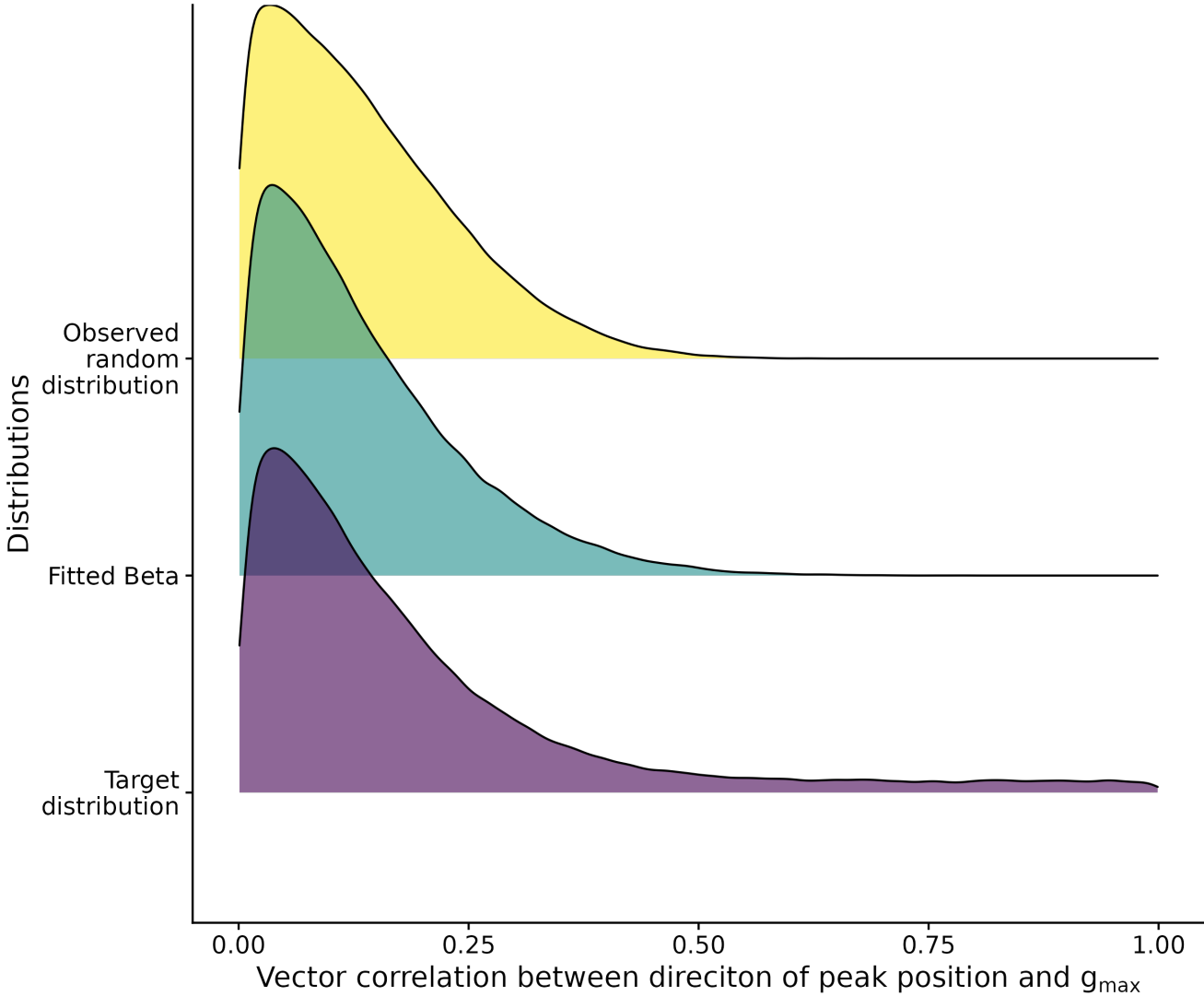


SI Figure 9: Simulations using random peaks. High-integration matrix is the Lutreolina P-matrix (eigenvalue variance=0.55), while the low-integration matrix is a modification of the Lutreolina P-matrix with eigenvalue variance of 0.01. The low-integration matrix has the same eigenvectors and total variance of the original matrix. We see a clear lack of Δz with high correlation to g_{max} . In these simulations, dimensionality of the phenotype is 35, and in the multi-peak landscape we have $N = 50$ peaks. Each dot corresponds to the final position of one of the 1000 simulated trajectories.

parameters a_r and b_r . This fitted beta distribution is then used in a mixture with a beta with parameters $a = 1$ and $b = 1$ and a mixture parameter ρ , which results in a target distribution of $Cor(\Delta z, g_{max})$ given by:

$$P(Cor(\Delta z, g_{max})) = \rho Beta(1, 1) + (1 - \rho)Beta(a_r, b_r)$$

Because $Beta(1, 1)$ is essentially flat in the $[0, 1]$ interval, this produces a small amount of vectors with correlations above 0.6, and this amount can be tuned by changing a and b or ρ . We select these parameters to produce a small amount of vectors in this region above 0.6, and to not change the rest of the distribution significantly. All three distributions (random, fitted beta, and enriched mixture) can be seen in SI Fig 10.



SI Figure 10: Comparison of the distributions of the correlations between peak position and g_{max} under the random distribution, the beta distribution fitted to this random distribution, and the target distribution using a mixture of betas. In this example: $a_r = 1.25$, $b_r = 8.05$, $\rho = 0.15$.

After determining the target distribution, we have to effectively sample the random peaks that follow this distribution. This is done using rejection sampling in three steps. First, we establish the number of random vectors we

want to sample and the precision we want the target distribution to be followed. This produces a target histogram for the random vectors, with a target number of vectors in each histogram bin. Table 1 shows an example of a histogram with 5 equally spaced bins and the corresponding number of vectors in each level of correlation that would need to be sampled. Next, we sample random vectors in the usual way, from a multivariate normal distribution, and fill as much of the target distribution as possible. Vectors whose correlation to g_{max} falls within one of the target bins that still have not been filled are accepted, while vectors falling into completely filled bins are discarded. This procedure mostly fills the bins with correlations lower than 0.5, but vectors with correlations above 0.5 are almost never observed. After this initial round of sampling, we generate random vectors with higher correlations to g_{max} by using perturbations. A perturbation vector is sampled from a multivariate normal distribution, and this perturbation vector is added to g_{max} . This produces a new random vector that can have its correlation to g_{max} tuned by altering the variance of the distribution that generates the perturbation. Small variances produce random vectors with higher correlation to g_{max} , while larger variances produce random vectors with lower correlations to g_{max} . By dynamically modifying this variance, we can complete the sampling of the target distribution and fill the bins with higher correlation to g_{max} . This pool of random directions that have been enriched to sample the region of high correlation with g_{max} is used to create the selective surface. The final position of the peaks is determined by sampling the distance of each peak from the origin from a uniform distribution, as described previously.

Table 1: Example target for the number of vectors in each correlation interval, for 5 intervals and 1000 vectors, using the distribution in SI Fig 10. In practice, we use many more intervals (30) and vectors (100000).

Correlation Interval	0-0.2	0.2-0.4	0.4-0.6	0.6-0.8	0.8-1
Number of vectors	684	212	58	22	24

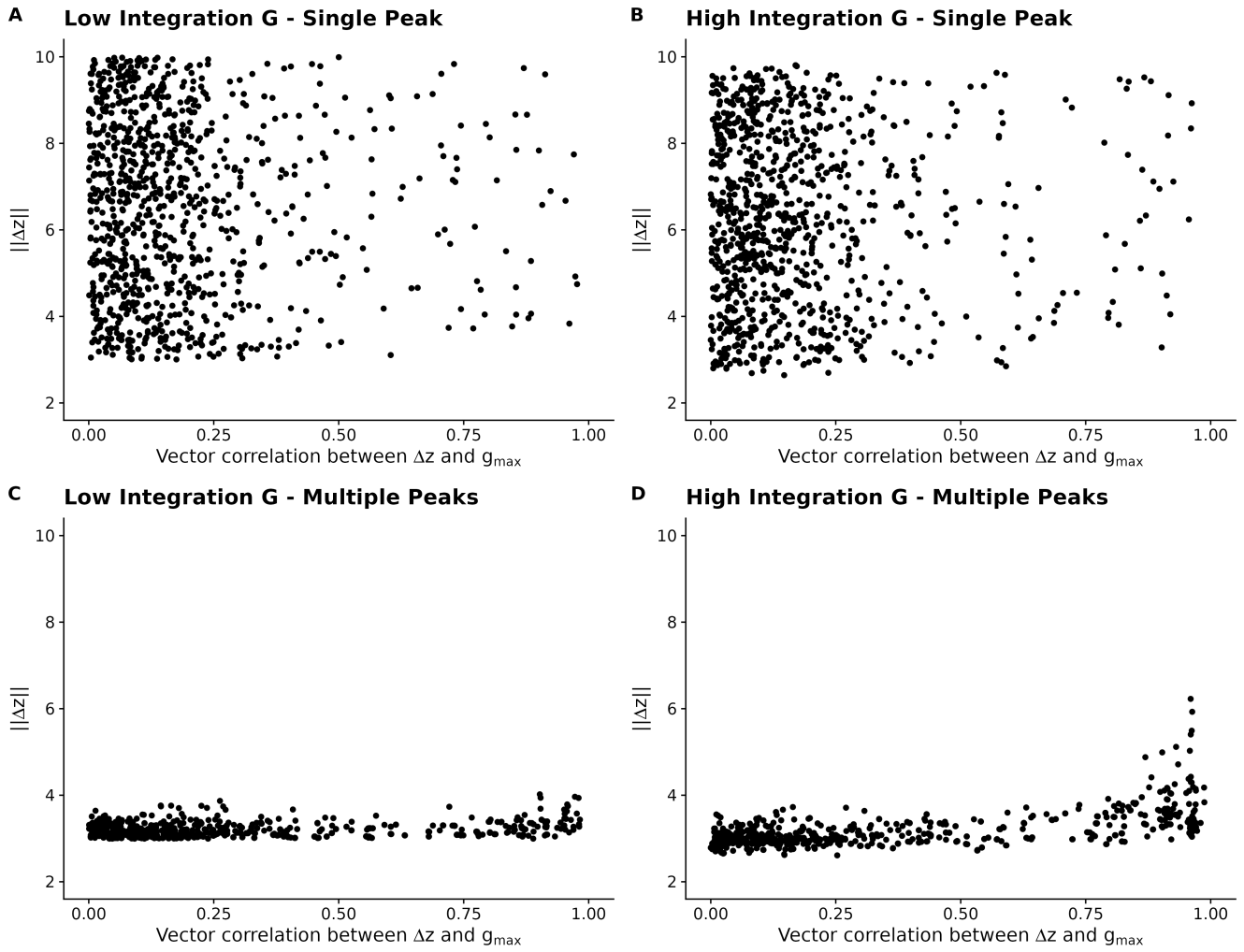
After enriching the peaks that are aligned with g_{max} , we can effectively investigate how the presence of these peaks affects the interaction between more or less integrated G-matrices and the selective surface. For the single peak landscapes, the results are similar to the random peaks, with the difference that we now observe some $Cor(\Delta z, g_{max})$ above 0.6, as expected. Still, for the single peak landscapes we see no difference between high- and low-integration G-matrices, and no relation between $Cor(\Delta z, g_{max})$ and Δz . For the multiple peak landscapes, the results are different, with the integrated G-matrix now showing an increase in $\|\Delta z\|$ for higher values of $Cor(\Delta z, g_{max})$. This pattern is similar to the one observed in natural populations.

Is it necessary for g_{max} to be related to size variation?

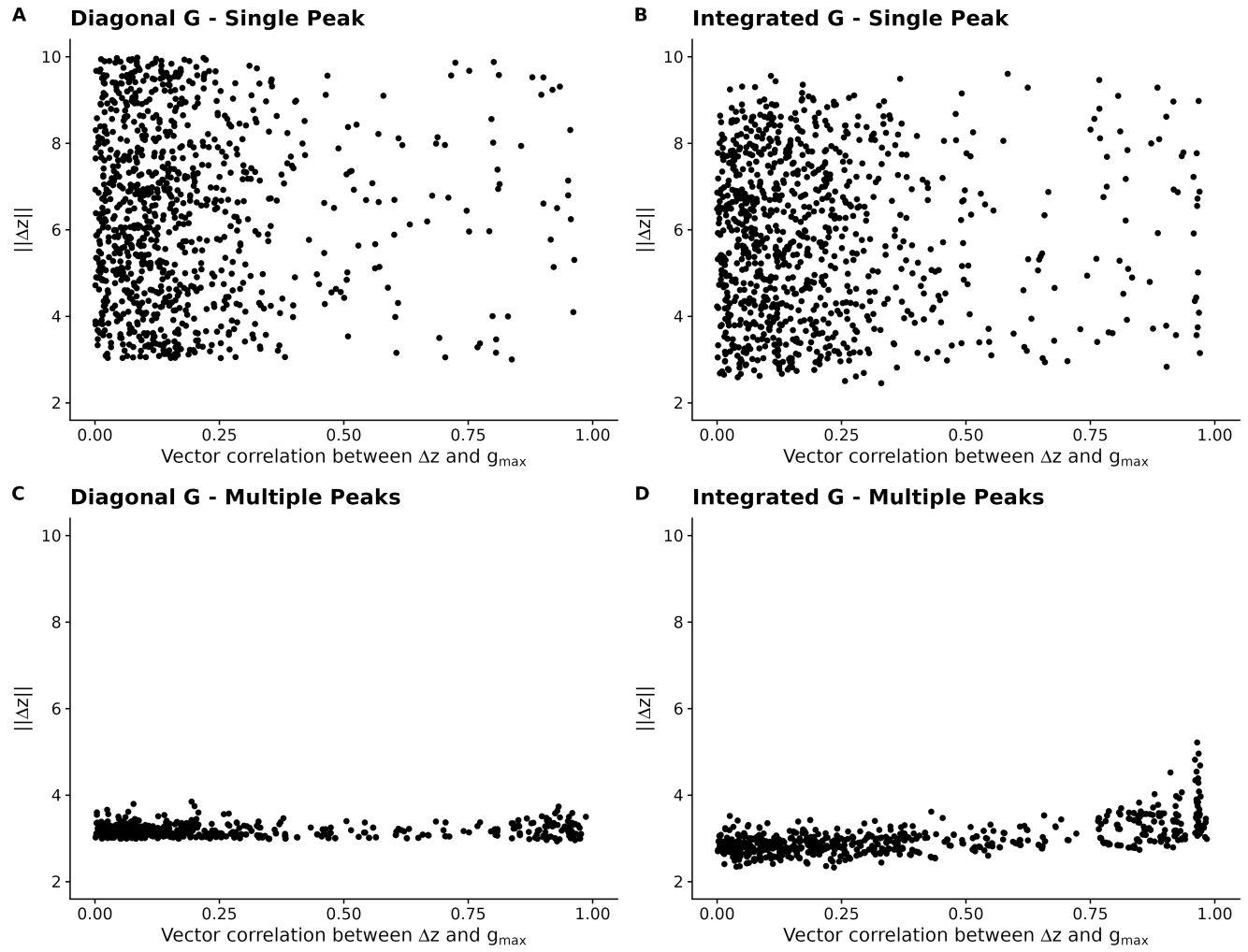
One possibility is that the effect we see in the increase of $\|\Delta z\|$ when the evolutionary response is aligned with g_{max} is due to the fact that the first principal component of the Lutreolina matrix is size related, and this biases the evolutionary response of the population in a way that is related to the global effect of size. To explore this possibility, we repeated the simulations using a P-matrix that has a first principal component that is **not** size related. For this, we choose the P-matrix from the bat species Ariteus flavescens (eigenvalue variance=0.13), whose first principal component is related too..., and the results (SI Fig 12) using this matrix are similar to the Lutreolina results (SI Fig 11), indicating that a size related g_{max} is not necessary for the covariance structure to bias the evolutionary response.

Discussion and Conclusions

We describe a simulation framework for investigating how populations with different levels of genetic integration evolve on complex fitness landscapes with multiple adaptive peaks. The simulations use a mixture of Gaussian functions to create selective surfaces with varying numbers of peaks. The change in mean phenotype of the population over time is modeled using the Lande equation, which incorporates the additive genetic covariance matrix



SI Figure 11: Simulations using a selective surface with an enriched number of peaks in the direction of g_{max} . High-integration matrix is the Lutreolina P-matrix (eigenvalue variance=0.55), while the low-integration matrix is a modification of the Lutreolina P-matrix with eigenvalue variance of 0.01. The low-integration matrix has the same eigenvectors and total variance of the original matrix. Compared to the results in SI Fig 9, we now see the increase in $\|\Delta z\|$ for high values of $Cor(\Delta z, g_{max})$ in the integrated matrix. In these simulations, dimensionality of the phenotype is 35, and in the multi-peak landscape we have $N = 50$ peaks. Each dot corresponds to the final position of one of the 1000 simulated trajectories.



SI Figure 12: Simulations using a selective surface with an enriched number of peaks in the direction of g_{max} for a species in which g_{max} is not size related.

(G-matrix) and the gradient of the fitness surface. The simulations explore the relationship between the magnitude of total phenotypic change ($\|\Delta z\|$) and evolutionary bias, the alignment between the direction of phenotypic change and the main axis of genetic variation in the populations $\text{Cor}(\Delta z, g_{max})$. To effectively sample the region of phenotype space aligned with g_{max} , we develop a sampling procedure that enriches the adaptive peaks in the direction of g_{max} .

The need for enrichment of peaks in the direction of g_{max} to observe the effect of genetic integration on the magnitude of phenotypic change ($\|\Delta z\|$) is an important result that suggests g_{max} itself may be a product of the evolution of the covariance structure. This finding has several implications for understanding the interplay between genetic architecture and adaptive landscapes in shaping evolutionary outcomes. First, the fact that randomly distributed peaks do not produce the observed relationship between $\text{Cor}(\Delta z, g_{max})$ and $\|\Delta z\|$ in highly integrated G-matrices suggests that the alignment between the main axis of genetic variation and the direction of selection is not a common occurrence under random conditions. The requirement for peak enrichment along g_{max} to observe this effect implies that the evolution of the G-matrix itself may be driven by the selective landscape. Over evolutionary time, the G-matrix may evolve in response to persistent selection pressures, leading to an alignment between the main axis of genetic variation (g_{max}) and the direction of selection. This alignment could be the result of a process of genetic accommodation, where the genetic architecture of a population evolves to better suit the selective pressures it experiences. In this scenario, g_{max} would represent an evolutionary “memory” of the past selective pressures that have shaped the covariance structure of the population. The evolution of g_{max} in response to selection could also explain why some empirical studies have found a relationship between Δz and g_{max} in across species divergence. If the G-matrix has evolved to align with the selective landscape, then the main axis of genetic variation would naturally be correlated with the direction of evolutionary change, leading to the observed pattern. Furthermore, the finding that the effect of genetic integration on $\|\Delta z\|$ does not depend on g_{max} being related to size variation suggests that the evolution of the G-matrix can be driven by a variety of selective pressures, not just those related to overall size. This highlights the complexity of the evolutionary process and the importance of considering the specific selective pressures acting on a population when studying the evolution of genetic architecture.

The simulations show that in multiple peak landscapes, the level of genetic integration in the G-matrix can influence the evolutionary trajectory and final phenotype of a population. For highly integrated G-matrices, there is an increase in the magnitude of phenotypic change ($\|\Delta z\|$) when the direction of evolutionary response is aligned with the main axis of genetic variation (g_{max}). This effect is not observed in single peak landscapes or for low-integration G-matrices. The findings suggest that the covariance structure of the G-matrix can bias the evolutionary response in a way that produces an observable signature in the divergence between species. Importantly, this effect does not depend on g_{max} being related to size variation, as similar results are obtained using a P-matrix with a first principal component unrelated to size. These simulations provide insights into how the microevolutionary interaction between genetic architecture and complex selective landscapes can shape macroevolutionary patterns.